Journal of Ceramic Processing Research. Vol. 18, No. 3, pp. 247~251 (2017)

J O U R N A L O F
Ceramic Processing Research

Electrical properties of Fe doped Ni-Mn-Co-O cubic spinel nanopowders for temperature sensors

Kyoung Ryeol Park[a,b], Sungwook Mhin[b], HyukSu Han[c], Kang Min Kim[c], Kwang Bo Shim[a], Jung-Il Lee[d] and Jeong Ho Ryu[d,*]

[a]*Department of Materials Science and Engineering, Hanyang University, Seoul 04763, Korea*
[b]*Korea Institute of Industrial Technology, Gaetbeol-ro 156, Yeonsu-gu, Incheon 21999, Korea*
[c]*Korea Institute of Industrial Technology, 137-41 Gwahakdanji-ro, Gangneung-si, Gangwon-do 25440, Korea*
[d]*Department of Materials Science and Engineering, Korea National University of Transportation, Chungju, Chungbuk 27469, Korea*

A sol-gel combustion process was used to synthesize $Fe_{0.48}Ni_{0.3}Mn_{1.32}Co_{0.9}O_4$ (FNMC) nanopowders, which exhibited properties suitable for negative temperature coefficient (NTC) thermistors. The chemical composition of the synthesized FNMC powder after calcination was within the expected values. Thermal analysis of the sol-gel synthesized nanopowders indicated that residual nitrate compounds volatilized and crystallization occurred during calcination. The influence of different calcination temperatures on the crystal structure of FNMC was investigated. A single-phase cubic spinel structure with improved crystallinity was observed after calcination at 1073 K. As expected, an increase in grain size up to 80 nm was observed with increasing calcination temperature. Elements such as Fe, Ni, Mn and Co were homogeneously distributed in both sol-gel synthesized nanopowders and calcined powders. Dense pellets of FNMC nanopowder were sintered at 1473 K in order to evaluate electrical properties. The electrical resistance (ρ_{20}) and B-value ($B_{20/80}$) were 0.36 kΩ and 3265 K, respectively, which are desirable values for an NTC thermistor. These results suggest that FNMC nanopowders show relatively stable electrical reliability because of the uniform microstructure and single-phase cubic spinel structure, making these nanopowders a suitable candidate for NTC thermistor materials.

Key words: Fe-Ni-Mn-Co-O, Single cubic spinel structure, Nanopowders, Thermistors, Sol-gel combustion.

Introduction

Negative temperature coefficient (NTC) thermistors used as temperature sensors and controllers have been widely studied because they are useful in many industrial and consumer applications, including the electronics, aerospace, and automotive industries [1]. Most NTC thermistors are composed of transition metal oxides with a spinel structure (AB_2O_4), which exhibits distinctive electrically semiconductive properties [2-4]. For example, in the case of nickel-cobalt manganite, electrical resistance decreases exponentially with increasing temperature. The conduction mechanism of the NTC thermistor can be described by phonon-assisted hopping between multi-valent cations on octahedral sites of the spinel structure. The hopping conduction arises from thermally induced lattice vibration, where the electrical conductivity reaches a maximum when the number of cations with a 3+ valence state equals that of cations with 4+ valence state [4-6].

The resistance of NTC thermistors can be further tailored to specific resistivity ranges by introducing transition metals (Fe, Cu, Al, Zn, etc.) as dopants in the spinel structure [4-9], and Fe is the most commonly chosen dopant in NTC thermistors [4, 8-11]. When Fe ions are introduced into Mn-Ni-Co-O, Fe ions randomly occupy tetrahedral or octahedral sites, which significantly alters cationic distributions and microstructures in the spinel structure. This leads to variations in the hopping distance, and is possibly related to the conduction mechanism [9-11].

The electrical performance and reliability of an NTC thermistor are a function of the crystal structure, microstructure, chemical composition, and elemental distribution, and all of these are dependent on powder synthesis techniques. To improve the performance of NTC, various processing methods have been explored, including co-precipitation [3, 4, 8], high-energy ball milling [12], and sol-gel combustion [5, 13, 14]. The co-precipitation method results in a very low yield compared to other synthesis techniques because pH control is difficult and varies based on the surface chemistry of each ceramic precursor [3, 15]. A high-energy ball milling process introduces chemical impurities from the collision between the inner walls of the milling jar and the ball mill media [16, 17]. The sol-gel combustion method is able to synthesize homogeneous nanopowders with precisely

*Corresponding author:
Tel : +82-43-841-5384, 82-10-3643-3466
Fax: +82-43-841-5380
E-mail: jhryu@ut.ac.kr

controlled chemical compositions at low processing temperatures [18].

Controlling the synthesis of single-phase nanopowders is important in applications such as NTC thermistors. In this study, Fe doped (Ni, Mn, Co)O_4 nanopowders, composed of a single-phase cubic spinel structure, was synthesized using a sol-gel combustion method. The effect of Fe doping on the crystallographic evolution and morphology of the nanopowders was studied using laboratory characterization techniques. In addition, FNMC nanopowders were sintered to high density, and the electrical properties of the ceramic were compared to those of typical NTC thermistors.

Experimental

FNMC $(Fe_{0.48}Ni_{0.3}Mn_{1.32}Co_{0.9})O_4$ nanopowders were prepared using a sol-gel combustion method. As precursors, stoichiometric nickel nitrate ($Ni(NO_3)_2 \cdot 6H_2O$), manganese nitrate ($Mn(NO_3)_2$, 50% aqueous solution), cobalt nitrate ($Co(NO_3)_2 \cdot 6H_2O$), and iron nitrate ($Fe(NO_3)_3 \cdot 9H_2O$) were dissolved in a mixture of water and ethylene glycol under constant stirring. Approximately 30 g (~ 1/6 mol) of citric acid was added to the solution while maintaining a constant temperature of 353 K. The pH of the solution was adjusted to ~ 6.8 by adding ammonium hydroxide (NH_4OH). The solution was stirred while heating to 453 K in order to transform the sol into a viscous gel. After 3-4 h, sol-gel combustion occurred and the gel transformed into fine powder.

The sol-gel synthesized nanopowders were calcined at different temperatures in air for 2 h, with a heating rate of 5 K/min. The calcined powder was mixed with a polyvinyl alcohol (PVA) organic binder solution. In order to form disk shaped pellets with a diameter of 14 mm and a thickness of 4 mm, 2.5 g of the powder was uniaxially pressed at 30 MPa. The green pellets were heated from room temperature to 873 K at a heating rate of 3 K/min, with a dwell time of 2 h in order to burn out the organic binder. The pellets were then heated to the sintering temperature of 1473 K with a heating rate of 4 K/min in air, and the sintering temperature for 4 h, and then cooled to room temperature.

The chemical composition of both the sol-gel synthesized nanopowders and the calcined powder were analyzed using X-ray fluorescence (XRF; ZSX-Primus, Rigaku) spectrometry. The microstructure and morphology of the FNMC nanopowders were observed using a field emission scanning electron microscope (FE-SEM; Nova Nano 450, FEI). Energy dispersive X-ray spectroscopy (EDS), coupled with the FE-SEM, was also utilized for elemental distribution mapping. Phase evolution and crystal structure of the obtained powders were characterized by X-ray diffraction (XRD; X'Pert-Pro MPD, PANalytical) using Cu Kα radiation at 40 kV and 30 mA. Fourier transform infrared spectroscopy (FT-IR; FT-IR 4600, JASCO) was used to investigate the formation of crystalline FNMC nanopowder. For measurement of electrical properties, silver paste was printed as electrodes on both sides of the sintered pellet, and then fired in a furnace at 900 K for 40 min. The temperature dependence of electrical resistance of FNMC pellets was measured in a silicon oil bath (G50, ThermoScientific, USA) by using a digital multimeter (RM 3545, HIOKI, Japan) increments of 10 K between 253 to 373 K.

Results and Discussions

The chemical composition of the FNMC powder was determined using XRF as shown in Table 1. A similar ratio among elements in FNMC (Fe : Mn: Ni : Co = 0.48 : 1.24 : 0.33 : 0.94) was obtained after the gel combustion process, as compared to the expected chemical composition (initial ratio in Table 1). Subsequent calcination of the sol-gel synthesized nanopowder at 1073 K for 2 h does not influence the chemical composition considerably. The XRF results indicate that the sol-gel combustion method can accurately control the chemical composition of the FNMC powder.

The microstructure and elemental distribution of both sol-gel synthesized nanopowders and calcined powders were examined using SEM and EDS. In Fig. 1(a), a secondary electron micrograph shows a reticular structure of particles with pores in the sol-gel synthesized nanopowder. This indicates that evaporation of the residual by-products occurs during combustion due to the ignition of the dried gel. The calcination process results in grain growth of the sol-gel synthesized nanopowder, confirmed by the observation of the spherical particles with sizes between 30 and 80 nm shown in Fig. 1(b). Elemental mapping of both synthesized nanopowders and calcined FNMC powders is shown in Fig. 1. Each element (Fe, Mn, Ni and Co) is homogeneously distributed over the sol-gel synthesized and calcined powders without elemental-rich and deficient regions, indicating that phase separation has not occurred during the combustion and calcination processes.

In order to confirm the formation of crystalline FNMC nanopowder, FT-IR spectra of the sol-gel synthesized and calcined powders were evaluated, as shown in Fig. 2. In the sol-gel synthesized nanopowder, the characteristic absorption peak was observed at

Table 1. Chemical compositions of FNMC nanopowders.

Elements	Chemical compositions		
	Initial ratio	As-burnt	Calcined at 1073 K
Fe	0.48	0.49	0.48
Mn	1.32	1.24	1.25
Ni	0.30	0.33	0.33
Co	0.90	0.94	0.94

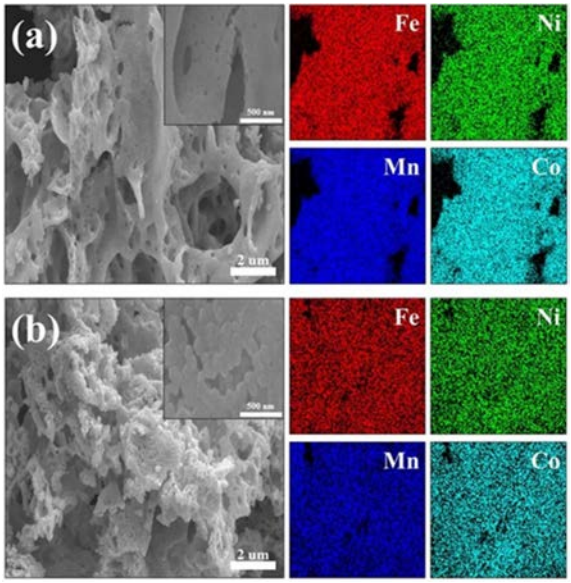

Fig. 1. SEM and EDS mapping (Fe, Ni, Mn and Co) images of FNMC nanopowders; (a) as-burnt, (b) calcined at 1073 K.

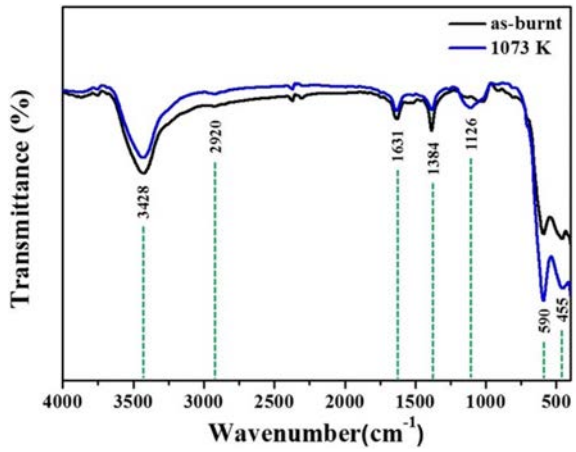

Fig. 2. FT-IR spectra of as-burnt and calcined FNMC nanopowders.

3428 cm^{-1}, attributed to the stretching mode of O-H bonds [19]. The absorption band at 2920 cm^{-1} can be interpreted as the stretching vibration of the CH_2 group [4, 19-21]. Absorption peaks at 1630 cm^{-1} and 1380 cm^{-1} correspond to the symmetric and asymmetric O-C-O stretching bonds, respectively, which can be closely related to residual organic compounds on FNMC nanopowders [8, 19-22]. After calcination of the sol-gel synthesized nanopowder, each absorption peak intensity related to the O-H and O-C-O bands is comparatively smaller due to the decomposition of the organic residuals during calcination. In particular, the absorption peak at 590 cm^{-1} is observed between 650 and 500 cm^{-1} associated with the coupling modes between the stretching vibration of Mn ions and –oxygen located at tetrahedral and octahedral sites [23]. The absorption peak at 455 cm^{-1} also indicates the stretching modes of the octahedral site; displacement of the Mn^{2+} ions in

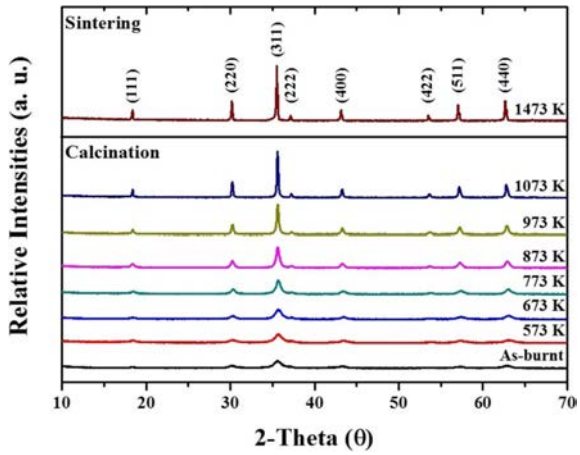

Fig. 3. XRD patterns of calcined and sintered FNMC nanopowders at different temperatures.

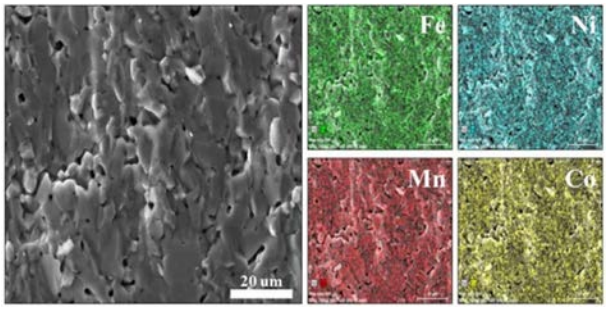

Fig. 4. A secondary electron micrograph of the surface, and EDS maps (Fe, Ni. Mn and Co) of the FNMC ceramic sintered at 1473 K.

tetrahedral sites is negligible [23-25]. Thus, the characteristic absorption peaks in the range between 400 and 600 cm^{-1} become more distinct, which is related to metal ions-to-oxygen bonding in the spinel structure. It is evident that the formation of a crystalline FNMC nanopowder occurs during calcination.

The crystal structure of the pellets sintered from synthesized FNMC nanopowders that were calcined at different temperatures was evaluated and the results are shown in Fig. 3. Diffraction peaks of the sol-gel synthesized nanopowder at 18.37, 30.24, 35.60, 37.23, 43.27, 53.61 and 57.16° can be assigned to the (111), (220), (311), (400), (422) and (511) of the cubic spinel structure ($Fd\bar{3}m$; JCPDS card No. 23-1237), respectively. Peak broadening in the diffraction patterns was observed at the lower temperatures, which is due to particle size effects or low crystallinity [26-28]. When the calcination temperature increases to 1073 K, the full width at half maximum (FWHM) of the diffraction peaks was significantly reduced and each diffraction peak becomes more distinct, implying that the calcination process promotes the crystallization of the FNMC nanopowders with a cubic spinel structure. After sintering at 1473 K, the cubic spinel phase was observed without secondary phases in the FNMC pellet, which implies that there is no structural change in FNMC

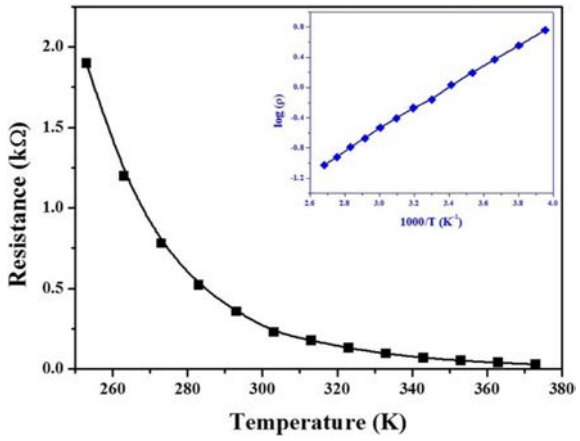

Fig. 5. Resistance vs. temperature plot of the FNMC ceramic sintered at 1473 K. The inset shows the relationship between log (ρ) with 1000/T (K^{-1}).

after sintering. Fig. 4 shows the microstructure of the sintered FNMC pellets, with elemental distribution mapping. Homogeneous distributions were observed for each element (Fe, Mn, Ni, and Co), implying that the sintering process does not lead to phase separation during high temperature heat treatment.

In order to evaluate the electrical properties of the sintered FNMC pellet to determine its suitability for NTC thermistor applications, the dependence of resistivity on the temperature was investigated. Resistance of the FNMC sample was measured as a function of temperature (253-373 K) and the result is displayed in Fig. 5. It was observed that the resistance of sintered FNMC pellets exponentially decreased with increasing temperature, which is a typical characteristic of semiconductive manganite spinel [29]. The thermal sensitivity factor for an NTC thermistor (B-value) can be estimated using the following equation;

$$R = R_0 \cdot exp\left(\frac{E}{k \cdot T}\right) = R_0 \cdot exp\left(\frac{B}{T}\right) \quad (1)$$

$$B = \frac{T_1 \cdot T_2}{T_2 - T_1} \cdot ln\left(\frac{R_1}{R_2}\right) \quad (2)$$

where E_a is the activation energy for hopping conduction, R is resistance, k is the Boltzman constant, and T is absolute temperature, respectively. Thus, the B-value can be obtained by calculating Eq. (2). As shown in Fig. 5 (inset), the relationship between log ρ and the reciprocal absolute temperature of the FNMC pellet represents a distinct linear relationship that is typical for NTC behavior [9]. The B value and room temperature resistance for the FNMC pellet were 3251 K and 0.359 kΩ, respectively. The B value of FNMC is comparable to that of $Mn_{3-x}Co_xO_4$ ($1.54 < x < 2.50$), which is known as a state-of-the-art NTC thermistor material. Also, the resistance and B-value in the range of 0-10 kΩ and 2000-7000 K, respectively, is favorable for most common NTC thermistor applications, indicating that sol-gel synthesized FNMC powder is a promising material for NTC thermistor application [1, 30].

Conlusions

$Fe_{0.48}Ni_{0.3}Mn_{1.32}Co_{0.9}O_4$ (FNMC) nanopowder was successfully synthesized via a gel combustion method. A single-phase cubic spinel structure was observed for the sol-gel synthesized FNMC nanopowder. As calcination temperature was increased to 1073 K, crystallinity of the FNMC powder improved and no secondary phases were observed. The chemical composition of the sol-gel synthesized nanopowders was maintained after calcination. Elemental distribution mapping revealed that each element (Fe, Mn, Ni and Co) was uniformly distributed over the microstructure of the powder after calcination as well as after sintering. A dense sintered FNMC ceramic pellet derived from the FNMC nanopowder was prepared to investigate its feasibility as a temperature sensor. A single-phase cubic spinel phase was observed for the sintered FNMC pellet, which implies that a phase transformation or segregation did not occur during the sintering process. The temperature dependent resistance variation of the FNMC follows typical behavior of semiconductive manganite spinel ceramics, which is demonstrated by the exponential decrease of resistance with increasing temperature. The room temperature resistance and B-value of the FNMC pellets were calculated as 0.359 kΩ and 3251 K, respectively. Based on these values, sintered FNMC material fabricated from sol-gel processed powders are suitable for NTC thermistor applications.

Acknowledgments

This research was supported by Basic Science Research Program through the National Research Foundation of Korea (NRF) funded by the Ministry of Education (No. 2016R1D1A3B03933765).

References

1. A. Feteira, Negative temperature coefficient resistance (NTCR) ceramic thermistors: An industrial perspective, J. Am. Ceram. Soc. 92 (2009) 967-983.
2. J.L. Martin De Vidales, P. Garcia-Chain, R.M. Rojas, E. Vila, O. Garcia-Martinez, J. Mater. Sci. 33 (1998) 1491-1496.
3. S.A. Kanade, V. Puri, Mater. Lett. 60 (2006) 1428-1431.
4. H. Zhang, A. Chang, C. Peng, Microelectron. Eng. 88 (2011) 2934-2940.
5. Z.X. Yue, J.H. Shan, X.W. Qi, X.H. Wang, J. Zhou, Z.L. Gui, L.T. Li, Mater. Sci. Eng., B 99 (2003) 217-220.
6. S. Jagtap, S. Rane, S. Gosavi, D. Amalnerkar, Preparation, J. Eur. Ceram. Soc. 28 (2008) 2501-2507.
7. K. Park, J.K. Lee, Scripta Mater. 57 (2007) 329-332.
8. J. Xia, Q. Zhao, A. Chang, B. Zhang, J. Alloys Compd. 646 (2015) 249-256.
9. R.N. Jadhav, S.N. Mathad, V. Puri, Ceram. Int. 38 (2012) 5181-5188.

10. M.N. Muralidharan, E.K. Sunny, K.R. Dayas, A. Seema, K.R. Resmi, J. Alloys Compd. 509 (2011) 9363-9371.
11. M.N. Muralidharan, P.R. Rohini, E.K. Sunny, K.R. Dayas, A. Seema, Ceram. Int. 38 (2012) 6481-6484.
12. J.A. Aguilar-Garib, F. Sanchez-de-Jesus, A.M. Bolarin-Miro, S. Ham-Hernandez, J. Ceram. Process. Res. 12(6) (2011) 721-726.
13. H. Zhang, A. Chang, F. Guan, L. Zhao, Q. Zhao, J. Yao, X. Huang, Ceram. Int. 40 (2014) 7865-7872.
14. W. Wang, X. Liu, F. Gao, C. Tian, Ceram. Int. 33 (2007) 459-462.
15. J.-W. Zhuang, A.-M. Chang, Z. Jia, S.-C. Zhuang, D.-Z. Jia, Ceram. Int. 30 (2004) 1661-1663.
16. C. Suryanarayana, Prog. Mater. Sci. 46 (2001) 1-184.
17. H.K. Han, C. Loka, Y.M. Yang, J.H. Kim, S.W. Moon, J.S. Cho, K.-S. Lee, J. Power Sources 281 (2015) 293-300.
18. M. Manso-Silvan, L. Fuentes-Cobas, R.J. Martin-Palma, M. Hernandez-Velez, J.M. Martinez-Duart, Surf. Coat. Technol. 151-152 (2002) 118-121.
19. S.-G. Wang, A.-M. Chang, H.-M. Zhang, Q. Zhao, Mater. Chem. Phys. 110 (2008) 83-88.
20. P.S. Kohli, P. Devi, P. Reddy, K.K. Raina, M.L. Singla, J. Mater. Sci.: Mater. Electron. 23 (2012) 1891-1897.
21. A. Ghasemi, M. Mousavinia, Ceram. Int. 40 (2014) 2825-2834.
22. M.A. Gabal, S.S. Ata-Allah, J. Phys. Chem. Solids 65 (2004) 995-1003.
23. M. Ishii, M. Nakahira, T. Yamanaka, Solid state Commun. 11 (1972) 209-212.
24. W.Z. Wang, C.K. Xu, G.H. Wang, Y.K. Liu, C.L. Zheng, Adv. Mater. 14 (2002) 837-840.
25. M. Stefanescu, M. Bozdog, C. Muntean, O. Stefanescu, T. Vlase, J. Magn. Magn. Mater. 393 (2015) 92-98.
26. Z.J. Zhang, Z.L. Wang, B.C. Chakoumakos, J.S. Yin, J. Am. Chem. Soc. 120 (1998) 1800-1804.
27. D.-Lai Fang, Z.-B. Wang, P.-H. Yang, W. Liu, C.-S. Chen, J. Am. Ceram. Soc., 89 [1] (2006) 230-235.
28. C. Ma, Y. Liu, Y. Lu, H. Gao, H. Qian, J. Ding, J. Mater. Sci.: Mater. Electron. 24 (2013) 5183-5188.
29. S. Guillemet-Fritsch, C. Chanel, J. Sarrias, S. Bayonne, A. Rousset, X. Alcobe, M.L. Martinez Sarrion, Solid State Ionics 128 (2000) 233-242.
30. K. Park, S.J. Yun, J. Mater. Sci.: Mater. Electron. 15 (2004) 259-362.